Journal of The Electrochemical Society, **157** (11) F159-F166 (2010)
0013-4651/2010/157(11)/F159/8/$28.00 © The Electrochemical Society

Electrochemical Characterization of Mixed Self-Assembled Films of Water-Soluble Single-Walled Carbon Nanotube-Poly(*m*-aminobenzene sulfonic acid) and Iron(II) Tetrasulfophthalocyanine

Bolade O. Agboola,[a] Jeseelan Pillay,[b,c] Katlego Makgopa,[b] and Kenneth I. Ozoemena[a,b,*,z]

[a]*Energy and Processes, Materials Science and Manufacturing, Council for Scientific and Industrial Research, Pretoria 0001, South Africa*
[b]*Department of Chemistry, University of Pretoria, Pretoria 0002, South Africa*
[c]*Mintek, Advanced Materials Division, Randburg 2125, South Africa*

The redox activities of water-soluble iron(II) tetrasulfophthalocyanine (FeTSPc) and single-walled carbon nanotube-poly(*m*-aminobenzene sulfonic acid) (SWCNT-PABS) adsorbed on a gold surface precoated with a self-assembled monolayer (SAM) of 2-dimethylaminoethanethiol (DMAET) have been described. Atomic force microscopy, cyclic voltammetry, and electrochemical impedance spectroscopy were employed to probe the buildup and formation of their thin solid films on the gold surface. The solid films exhibited excellent electrochemical stability. The electrode based on the mixed hybrids (Au-DMAET-SWCNT-PABS/FeTSPc) exhibited the fastest electron transport ($k^o \approx 0.4$ cm s^{-1}) compared to other electrodes (~ 0.2 cm s^{-1}), suggesting the ability of the SWCNT-PABS to act as efficient conducting species that facilitate electron transport between the integrated FeTSPc and the underlying gold substrate. Given the paucity of literature in the SAMs of water-soluble phthalocyanine complexes, the proposed fabrication strategy could potentially be extended to other water-soluble metallophthalocyanines and related organometallic complexes.
 [DOI: 10.1149/1.3481410]

Manuscript submitted March 17, 2010; revised manuscript received June 1, 2010. Published September 1, 2010.

The smart immobilization of ultrathin solid films of nanomaterials on a solid surface has continued to attract major research interest because of the potential to open up a wide range of diverse technological and engineering applications. In this regard, the immobilization of materials on electrode surfaces using the conventional self-assembly strategy[1-5] and its related layer-by-layer (LBL) self-assembly[6-8] has continued to receive considerable attention. The self-assembly method is advantageous because of its simplicity and control of the order of material buildup, which might allow a synergic relationship between the materials toward specific purposes. In this respect, works on functionalization of carbon nanotubes (CNTs) to suit specific purposes have been on rapid increase. CNTs are suitable candidates for various applications due to their unique physical and chemical properties.[9,10] Transition-metal phthalocyanines (MPc's) have continued to be very relevant in their applications as suitable materials in various technological relevant applications, for example, in photocatalytic[11,12] and electrochemical sensing[13-20] owing to their excellent physicochemical properties.[21-23]

Transition-metal tetrasulfophthalocyanine (MTSPc, where M = central metal ion) complexes, notably iron(II) tetrasulfophthalocyanine (FeTSPc, Fig. 1a), are highly water-soluble species and well recognized for their high catalytic activity in homogeneous electrocatalysis. The ease with which they are washed away from electrodes during electrochemical studies has long been a major setback and has limited their fundamental studies and potential applications for heterogeneous electrocatalysis in an aqueous environment. The immobilization of sulfonated MPc complexes onto electrodes has to be assisted by redox-active polymeric complexes.[17] To date, all available papers on the surface confinement of water-soluble MTSPc complexes involved indium tin oxide-coated glass electrodes and LBL strategy using polycationic and/or highly branched polymeric complexes such as polyamidoamine (PAMAM) dendrimers,[8] chitosan,[24] and PAMAM.[25] Francisco Silva and co-workers[26] reported the use of drop-casting to immobilize a slurry of NiTSPc and SWCNTs onto a glassy carbon electrode (GCE). The most common feature of the LBL strategies include the use of a cocktail of relatively expensive reagents and the confinement of the MTSPc inside the thick multilayered polymeric films. The main problems usually associated with physical anchorage (i.e., the drop-casting method) of such films onto a GCE surface are poor stability as well as the difficulty in controlling the amount of film or thickness deposited. These problems have the tendency to compromise on the application of the films. It is very crucial to continue the search for other means of immobilizing them onto electrode surfaces as thin stable solid films without compromising on their electrocatalytic activity toward the detection of analytes in aqueous conditions. More importantly, integrating such water-soluble redox-active MPc complexes with CNTs (as electron transfer mediators) could provide an interesting synergistic means of further enhancing the electron transfer dynamics of MPc complexes. Our group[27-30] and others[8,26] have shown the feasibility of integrating CNTs and MPc complexes for enhanced electrochemical properties, but the use of water-soluble MPc complexes for this type of work is rarely reported.

This study reports the integration of FeTSPc (Fig. 1a) and single-walled carbon nanotube-poly(*m*-amino benzene sulfonic acid) (SWCNT-PABS, Fig. 1b), singly or as mixed, immobilized onto a gold electrode via an electrostatic interaction self-assembly strategy using a positively charged 2-dimethylamino-ethanethiol (DMAET) self-assembled monolayer (SAM) as the base coordinating species. We clearly proved that when these water-soluble FeTSPc and SWCNT-PABS are confined on the gold surface using the proposed strategy, they exhibit excellent electrochemical stability. To provide some understanding on the redox behavior, we explored the electron transfer dynamics of the modified electrodes using electrochemical impedance spectroscopy (EIS) and cyclic voltammetry (CV).

Experimental

Materials and reagents.— FeTSPc (Fig. 1a) was synthesized following the well-established Weber and Busch strategy.[31] SWCNT-PABS (Fig. 1b) and DMAET ($HS(CH_2)_2N^+H(CH_3)_2Cl^-$) were obtained from Aldrich. Epinephrine and *N*,*N*-dimethylformamide (DMF) were purchased from Sigma-Aldrich; DMF was distilled and dried before use. Potassium hexacyanoferrate(II) was obtained from B. Jones Ltd., SA. Potassium hexacyanoferric(III) was purchased from Bio-Zone Chemicals, SA. Ultrapure water of resistivity 18.2 MΩ cm was obtained from a Milli-Q Water System (Millipore Corp. Bedford, MA) and was used throughout for the

* Electrochemical Society Active Member.
z E-mail: kozoemena@csir.co.za

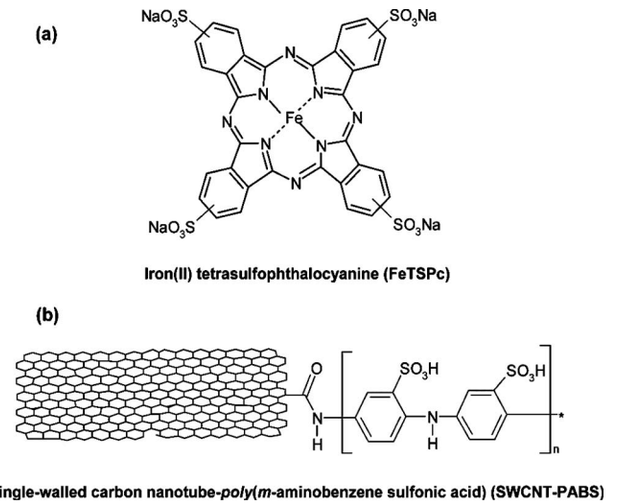

Figure 1. Molecular structures of (a) FeTSPc and (b) SWCNT-PABS.

preparation of solutions. KH_2PO_4 and K_2HPO_4 were used to prepare phosphate buffer solutions (PBSs) of the required pH. All electrochemical experiments were carried out in nitrogen atmosphere. All other reagents were of analytical grade and were used as received from the suppliers without further purification.

Apparatus and procedure.— Electrochemical studies were carried out using an Autolab potentiostat PGSTAT 302 (Eco Chemie, Utrecht, The Netherlands) driven by the General Purpose Electrochemical Systems data processing software (version 4.9). The working electrode was bare Au or the same Au electrode modified. Ag | AgCl, saturated KCl reference, and platinum wire counter electrodes were employed. EIS measurements were performed with Autolab FRA software between 1.0 Hz and 10 kHz using a 5 mV root-mean-square sinusoidal modulation. A complex nonlinear least-squares method based on the EQUIVCRT program[32] was used for automatic fitting of the obtained data. A further useful feature of the FRA software is its Kramers–Kronig rule check option. All recorded impedance data were subjected to this consistency check (low χ^2 values) to establish if the recorded spectra could be fitted to equivalent circuits and were rejected if they failed the test. All pH measurements were performed using a Labotec Orion bench top pH meter model 420A. Atomic force microscopy (AFM) experiments were performed with an AFM 5100 System (Agilent Technologies) using a contact mode AFM scanner interfaced with a Picoview 1.4.3 controller (scan range 1.25 μm in *x*-*y* and 2.322 μm in *z*). Silicon-type PPP-CONT-20 (Nanosensors) of thickness 2.0 ± 1.0 μm, length 450 ± 10 μm, width 50 ± 7.5 μm, spring constants 0.02–0.77 N m^{-1}, resonant frequencies of 6–21 kHz and tip height of 10–15 μm were used. All images (256 samples/line $\times$ 256 lines) were taken in air at room temperature and at scan rates 0.5–0.6 lines s^{-1}.

Immobilization of FeTSPc and SWCNT-PABS on gold electrode.— Before the experiments, the gold electrode was first cleaned using slurries of aluminum oxide nanopowder (Sigma-Aldrich), mirror-finished on a Buehler felt pad, and then subjected to ultrasonic vibration in ethanol to remove residual alumina nanopowder at the surface. The gold electrodes were then treated with the "Piranha" solution [1:3 (v/v) 30% H_2O_2 and concentrated H_2SO_4] for ~2 min; this step was necessary to remove organic contaminants and was followed by thorough rinsing with distilled water and ethanol. The gold electrode was finally cleaned electrochemically by carrying out CV experiments in 0.5 M H_2SO_4 and scanning the potential between −0.5 and 1.5 V (vs Ag | AgCl, saturated KCl) at a scan rate of 0.05 V s^{-1} until the 50th scan when a reproducible CV scan was obtained.

The electrode was again rinsed with absolute ethanol and immediately placed into a nitrogen-saturated absolute ethanol solution of 5 mM DMAET for 36 h in the dark to form a DMAET SAM bold electrode (Au-DMAET). Thereafter, the electrode was thoroughly rinsed in ethanol to remove weakly adsorbed DMAET molecules, dried in stream of nitrogen, and immediately immersed in a nitrogen purged 10 mL aqueous solution of 4 mg FeTSPc (to obtain the electrode herein abbreviated as Au-DMAET-FeTSPc) or a 10 mL aqueous solution of 4 mg SWCNT-PABS (to form the electrode, Au-DMAET-SWCNT-PABS) or their mixtures (to form the electrode abbreviated as Au-DMAET-SWCNT-PABS/FeTSPc). Each of the electrodes was kept in the dark and left for 6 h for the attachment of negatively charged FeTSPc and SWCNT-PABS onto the preformed positively charged Au-DMAET by electrostatic attraction. At short deposition times (<6 h), we did not see a significant response of the Fe(II)Pc/Fe(III)Pc couple. Because the theme of the work was to observe the electrochemistry of the adsorbed redox species, all studies were performed at a longer deposition time. After the formation of FeTSPc and SWCNT-PABS layers, the modified electrodes were then thoroughly rinsed with water and dried gently in a weak flowing nitrogen gas. When not in use, the modified electrodes were stored in a nitrogen-saturated phosphate buffer solution (pH 7.4) at room temperature. Any buffer solution of acidic or neutral pH can be used for this purpose; basic conditions may desorb the modifier.

The real surface area of the bare gold electrode was determined using the Randles–Sevcik equation (Eq. 1) for reversible, diffusion-controlled electrochemistry[33,34]

$$I_{pa} = (2.69 \times 10^5) n^{3/2} A D^{1/2} C \nu^{1/2} \quad [1]$$

where n is the number of electrons involved ($n = 1$ in the $[Fe(CN)_6]^{3-/4-}$ redox system), A is the geometric area of the electrode (0.020 cm^2), D is the diffusion coefficient of the $[Fe(CN)_6]^{3-/4-} = 7.6 \times 10^{-6}$ cm^2 s^{-1},[33] and $C = 1.0 \times 10^{-6}$ mol cm^{-3} is the bulk concentration of $[Fe(CN)_6]^{3-/4-}$. From the slope of the linear plot of the anodic peak current (I_{pa}) vs the scan rate ($R^2 > 0.99$, passing through the zero point), the experimentally determined surface area (A) was 0.026 cm^2, giving a surface roughness factor of 1.28 (ratio of real to geometrical surface area).

Results and Discussion

Electrode fabrication and AFM characterization.— Scheme 1 represents the self-assembly fabrication of the various electrodes via a strong electrostatic interaction between the positively charged DMAET and the negatively charged FeTSPc and SWCNT-PABS species. The buildup and formation of the films on gold plates were confirmed using the AFM technique. Figure 2 shows the comparative AFM images of Au-DMAET (Fig. 2a), Au-DMAET-FeTSPc (Fig. 2b), Au-DMAET-SWCNT-PABS (Fig. 2c), and Au-DMAET-SWCNT-PABS/FeTSPc (Fig. 2d). There was no significant difference between the topography thickness of the bare Au (not shown) and Au-DMAET, which is expected for this short-chained alkanethiol SAM as other workers[35] too did not even observe any difference between bare Au and on modification with a long-chained SAM of 11-amino-1-undecanethiol. Also, the roughness profiles increase as 1.43, 3.33, 3.85, and 5.71 for Au-DMAET, Au-DMAET-FeTSPc, Au-DMAET-SWCNT-PABS, and Au-DMAET-SWCNT-PABS/FeTSPc, respectively.

CV in aqueous (pH 7.4) conditions.— Figure 3 compares the cyclic voltammograms of (i) Au-DMAET, (ii) Au-DMAET-SWCNT-PABS, (iii) Au-DMAET-FeTSPc, and (iv) Au-DMAET-SWCNT-PABS/FeTSPc in 0.05 M PBS (pH 7.4) recorded at 0.050 V s^{-1}. The weak reversible process shown by Au-DMAET is attributed to the electric-field driven protonation/deprotonation process.[36,37] The CV of Au-DMAET is well-defined only when less deposition time (≤24 h) and/or a slightly lower concentration of DMAET (<5 mM) is used in the fabrication, as observed in the

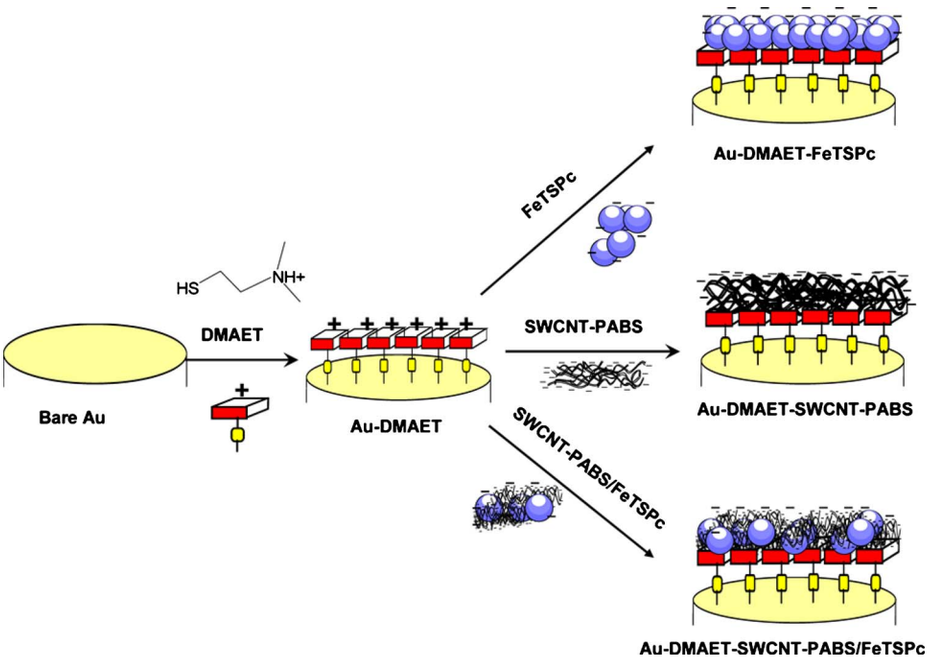

Scheme 1. Schematic representation of the fabrication route for the modified electrodes.

previous papers.[37] In this work, longer deposition times (~36 h) and a slightly higher concentration (5 mM) of DMAET was employed to ensure complete coverage of the base gold electrode. Both Au-DMAET-FeTSPc and Au-DMAET-SWCNT-PABS/FeTSPc showed well-defined reversible peaks, attributed to the Fe^{2+}/Fe^{3+} redox processes.[38] The ratio of the anodic and cathodic peak current densities (I_{pa}/I_{pc}) is approximately unity, indicating electrochemical reversibility. Figure 4a and b is the cyclic voltammograms obtained at different scan rates (0.025–1.0 V s^{-1} range) in a phosphate buffer pH 7.4 solution obtained at Au-DMAET-FeTSPc and Au-DMAET-SWCNT-PABS/FeTSPc, respectively. At a scan rate of 50 mV s^{-1}, the formal potentials (i.e., $E_{1/2} = [E_{pa} + E_{pc}]/2$) of Au-DMAET-FeTSPc and Au-DMAET-SWCNT-PABS/FeTSPc are 170 and 220 mV, respectively (Table I). Ideally, at small scan rates, the

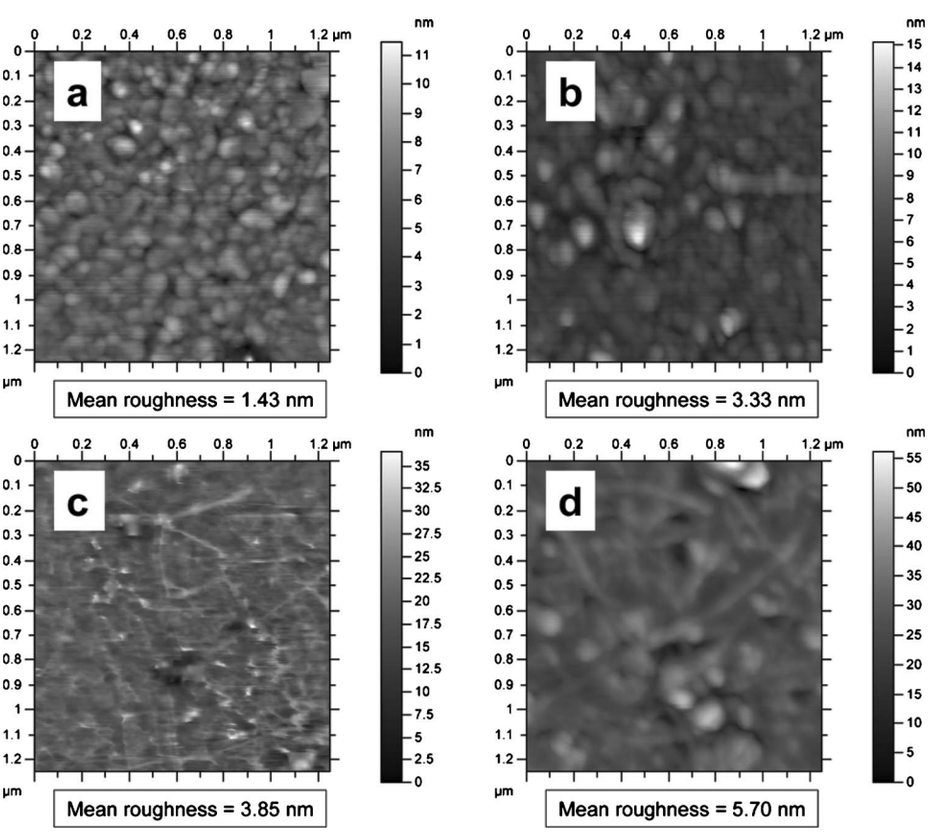

Figure 2. AFM images for (a) Au-DMAET, (b) Au-DMAET-FeTSPc, (c) Au-DMAET-SWCNT-PABS, and (d) Au-DMAET-SWCNT-PABS/FeTSPc.

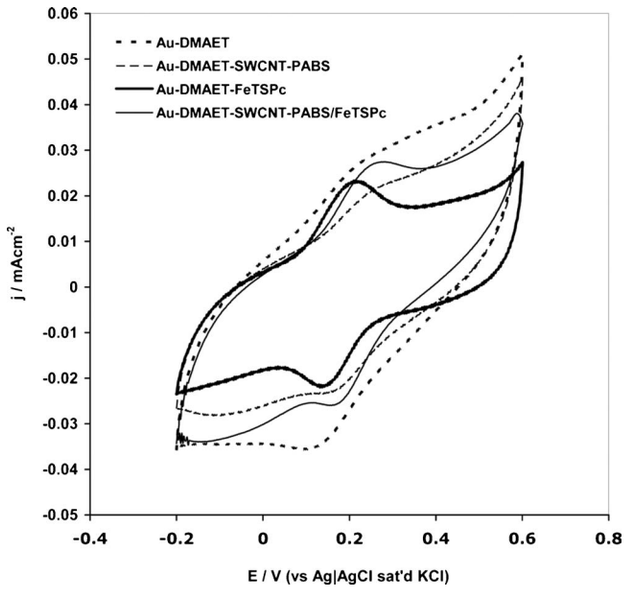

Figure 3. Comparative cyclic voltammograms in phosphate buffer pH 7.4 solution obtained at the various electrodes. Scan rate = 50 mV s^{-1}.

peak-to-peak potential separation ($\Delta E_p = |E_{pa} - E_{pc}|$) in a monolayer should be 0 V. However, as seen from Table I, the ΔE_p values for Au-DMAET-FeTSPc and Au-DMAET-SWCNT-PABS/FeTSPc are 78 and 112 mV, respectively. At higher scan rates (>0.5 V s^{-1}), the ΔE_p values for Au-DMAET-FeTSPc and Au-DMAET-SWCNT-PABS/FeTSPc are 142 and 133 mV, respectively. Thus, unlike at a low scan rate, the electron transport (signified by the magnitude ΔE_p) is slightly slower at Au-DMAET-FeTSPc than at Au-DMAET-SWCNT-PABS/FeTSPc at a high scan rate. This behavior is known to be due to an uncompensated resistance rather than a quasi-reversible electron transfer.[7] Also, the width at half the peak current (E_{fwhm}/mV) (where fwhm is full width at half-maximum) slightly deviate from the ideal value of 90.6/n mV for $n = 1$,[39-43] with Au-DMAET-FeTSPc and Au-DMAET-SWCNT-PABS/FeTSPc at 122 and 127 mV, respectively. The deviation of the ΔE_p and E_{fwhm} from their ideal values is typical of redox species being located in different environments with different formal potentials.[43-46] Thus, the FeTSPc molecules are located at different environments with different formal potentials. Simply stated, the FeTSPc species have different formal potentials when immobilized at DMAET and/or SWCNT-PABS and, thus, the effective voltammetric wave consists of a superposition of distinct electrochemical responses, resulting in the observed nonideal voltammograms. In all cases, the electrochemical parameters of DMAET-FeTSPc are slightly better than those recorded for SWCNT-PABS/FeTSPc, and this should not be totally surprising considering the different environments and complexity of the SWCNT-PABS platform.

The surface concentration of the immobilized FeTSPc species was determined using the conventional equation (Eq. 2)

$$\Gamma = \frac{Q}{nFA} \quad [2]$$

where Γ is the surface concentrations in mol cm^{-2}, Q is the integrated area of the anodic or cathodic charge, n is the number of electrons transferred (=1), F is Faraday's constant, and A is the electrode surface area. The surface concentrations were estimated to be $\sim 1.3 \times 10^{-9}$ and 1.4×10^{-9} mol cm^{-2} for Au-DMAET-FeTSPc and Au-DMAET-SWCNT-PABS/FeTSPc, respectively (Table I). The estimated values indicate multilayer coverages rather than a monolayer concentration expected to be in the order of $\sim 10^{-10}$ mol cm^{-2} for MPc molecules.[2,19,47,48]

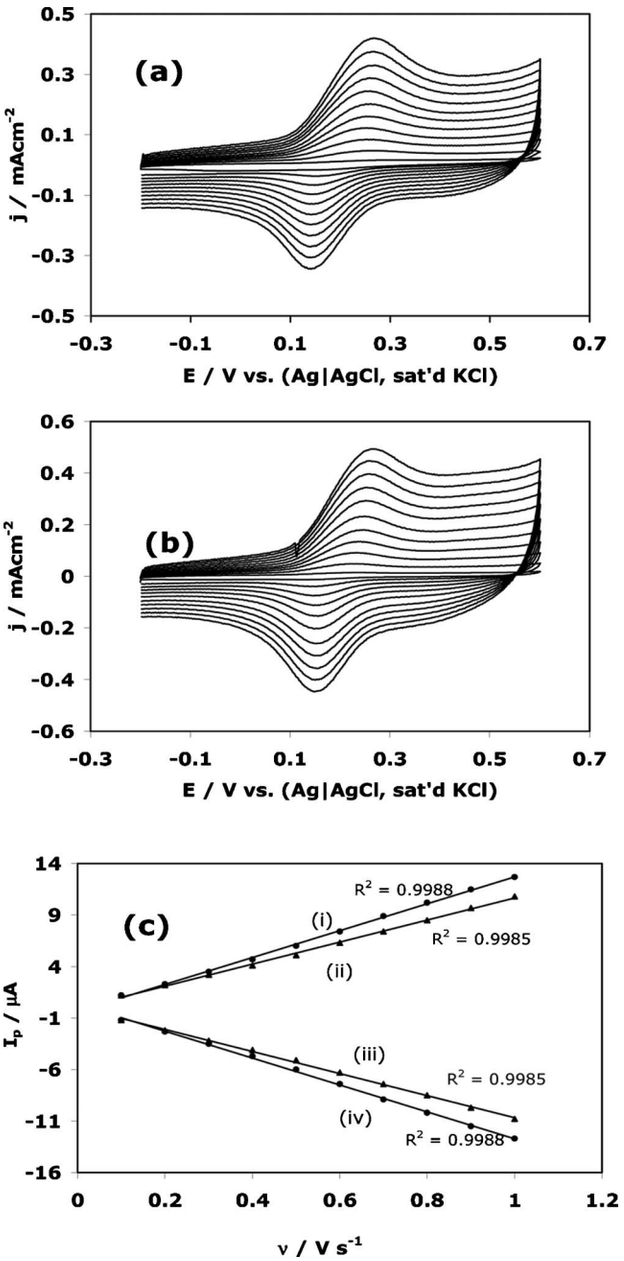

Figure 4. Cyclic voltammograms obtained at different scan rates (0.025–1.0 V s^{-1} range) in phosphate buffer pH 7.4 solution obtained at (a) Au-DMAET-FeTSPc and (b) Au-DMAET-SWCNT-PABS/FeTSPc. (c) represents the plots of anodic (i and ii) and cathodic (iii and iv) peak current response vs scan rate for the SWCNT-PABS/FeTSPc (i and iii) and DMAET-FeTSPc (ii and iv).

Insights into the capacitive behavior of the modified electrodes (C_{dl}/F cm^{-2}) may be estimated in the nonfaradaic regimes (−0.1 V vs Ag/AgCl) using Eq. 3[29,49]

$$C_{dl} = \frac{I_{ch}}{\nu A} \quad [3]$$

where I_{ch} is the charging current, ν is the scan rate, and A is the calculated area of the electrode (0.026 cm^2 for Au-DMAET and Au-DMAET-FeTSPc, 0.028 cm^2 for Au-DMAET-SWCNT-PABS, and ~0.030 cm^2 for Au-DMAET-SWCNT-PABS/FeTSPc). The capacitance decreased as Au-DMAET (692 µF cm^{-2})

Table I. Summary of cyclic voltammetric data obtained at the FeTSPc-based electrodes. Scan rate = 50 mV s^{-1}.

	FeTSPc-based electrodes	
Parameter	Au-DMAET-FeTSPc	Au-DMAET-SWCNT-PABS/FeTSPc
Γ/mol cm^{-2}	$(1.31 \pm 0.11) \times 10^{-9}$	$(1.38 \pm 0.11) \times 10^{-9}$
$E_{1/2}$/mV	170	220
ΔE_p/mV	78	122
E_{fwhm}/mV	112	127

> Au-DMAET-SWCNT-PABS/FeTSPc (660 μF cm^{-2}) > Au-DMAET-SWCNT-PABS (552 μF cm^{-2}) > Au-DMAET-FeTSPc (404 μF cm^{-2}). The trends may explain the ability of the electrodes to store charges/electrolyte ions within the porous layers.

For a surface-confined species, the peak current is directly proportional to the scan rates, agreeing with Eq. 4[34,39,40]

$$I_p = \frac{n^2F^2A\Gamma\nu}{4RT} \quad [4]$$

where R is the ideal gas constant, T is the absolute temperature (K), and the other symbols retain their usual meaning. As expected from Eq. 4, the plots of the peak currents (I_p) against the scan rate (ν) are linear (Fig. 4c).

Further, we investigated the electrochemical stability of Au-DMAET-FeTSPc and Au-DMAET-SWCNT-PABS/FeTSPc by repetitively scanning each electrode in PBS (pH 7.4). The repetitive cycling of Au-DMAET-FeTSPc and the comparative CVs of freshly prepared and after 1 week of use in PBS is shown in Fig. 5a and b, respectively. Figure 5a shows that in terms of I_p and E_p, the CV pattern did not significantly change with repeated cycling and upon comparing the CVs (Fig. 5b) of the freshly prepared Au-DMAET-FeTSPc with that of a week old. Au-DMAET-FeTSPc/SWCNT-PABS also showed the same stability (not shown) as Au-DMAET-FeTSPc. Such remarkable stability is important for their electrochemical studies as well as their potential applications in aqueous conditions. This result is remarkable because FeTSPc is highly soluble in water but on its attachment to Au-DMAET film, it bonds very strongly by an electrostatic attraction between SO_3^- of FeTSPc and $NH^+(CH_3)_2$ of SWCNT-PABS, and this bond is stable even when the electrode is used in aqueous media.

Impedimetric study in $[Fe(CN)_6]^{4-}/[Fe(CN)_6]^{3-}$ solution.— Next, we sought to establish the extent to which the modifying species permit the electron transfer of the $[Fe(CN)_6]^{4-}/[Fe(CN)_6]^{3-}$ redox probe to the underlying gold electrode. The electrolyte was 1 mM $[Fe(CN)_6]^{4-}/[Fe(CN)_6]^{3-}$ in 0.1 M KCl. As seen in Fig. 6, with the exception of Au-DMAET-SWCNT-PABS/FeTSPc that give higher anodic and cathodic peak currents, the CV responses of the electrodes were essentially the same in terms of (*i*) peak-to-peak separation potential ($\Delta E_p \approx 70$ mV vs Ag | AgCl, saturated KCl) and (*ii*) the equilibrium potential ($E_{1/2} \approx 0.25$ V vs Ag | AgCl, saturated KCl). Also, Au-DMAET-FeTSPc and Au-DMAET-SWCNT-PABS/FeTSPc did not show any significant CV responses in 0.1 M KCl solution, clearly suggesting that the surface-confined FeTSPc complex does not play any detectable role in the observed electrochemistry of $[Fe(CN)_6]^{4-}/[Fe(CN)_6]^{3-}$ in the experimental conditions employed here. Thus, all further experiments were devoted to the KCl solution containing the redox probe.

To follow the electron transfer kinetics occurring at these electrodes, we employed EIS because this technique easily provides a full description of the electrochemical system compared to CV.[50] From a recent work,[28] there was no significant difference when the experiment was conducted at or less than 1 Hz; thus, all EIS experiments here were carried out at a minimum frequency of 1 Hz. The experimental impedance spectra yielded values for χ^2 in the range

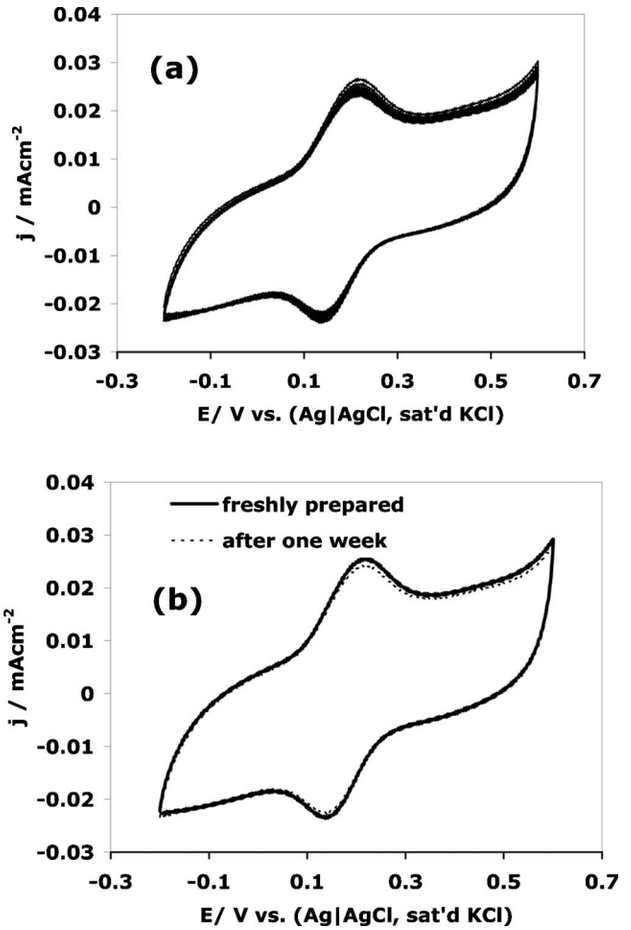

Figure 5. (a) Cyclic voltammogram evolution for the repetitive cycling obtained in PBS at Au-DMAET-FeTSPc and (b) CVs obtained at (i) freshly prepared Au-DMAET-FeTSPc and (ii) a week after use. Scan rate = 50 mV s^{-1}.

between 10^{-6} and 10^{-5} from the Kramers–Kronig tests, indicating satisfactory results. The spectra (Nyquist plots) are compared in Fig. 7 and were fitted using the modified Randles' equivalent circuits (Fig. 7 inset) involving the uncompensated or solution resistance (R_s), electron transfer resistance (R_{ct}), constant phase element (CPE), and Warburg-type impedance (Z_w), which are associated with the domain of mass transport control arising from the diffusion of ions to and from the electrode|solution interface. The slopes of the Warburg lines of the spectra are approximately 1, agreeing with the literature for a well-behaved Warburg impedance, which are characterized by straight lines with slopes of 1.[51] The heterogeneous electron transfer rate constant (k^o) values of the electrodes were obtained from the equation[34,51]

$$k^o = \frac{RT}{n^2F^2AR_{ct}C} \quad [5]$$

where n is the number of electrons transferred (3), C is the concentration of $[Fe(CN)_6]^{4-}/[Fe(CN)_6]^{3-}$ (1×10^{-6} mol cm^{-3}), R, T, F, and A have their usual meaning, and R_{ct} is the charge-transfer resistance. The following features shown by the impedimetric data of the modified electrodes should be emphasized. First, from the data in Table I, Au-DMAET-SWCNT-PABS/FeTSPc gave the highest k^o value, indicating that charge-transfer processes between $[Fe(CN)_6]^{3-/4-}$ and the underlying gold surface are made much easier by the synergistic combination of FeTSPc and SWCNT-

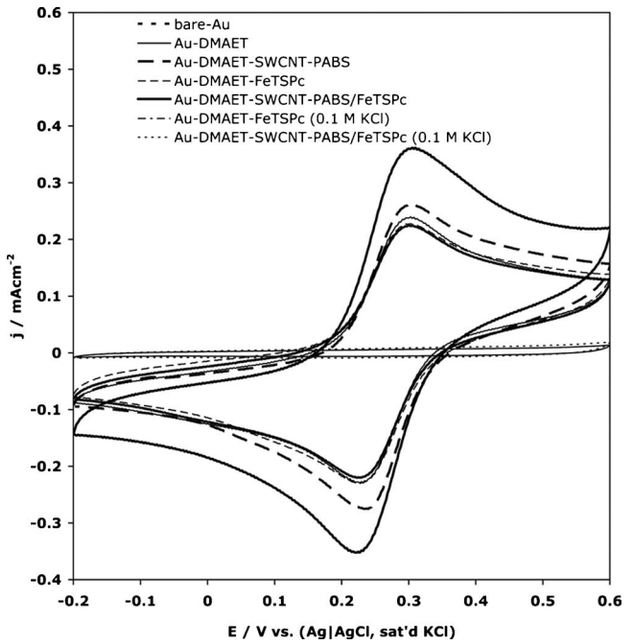

Figure 6. Cyclic voltammograms obtained at the electrodes in 1 mM $[Fe(CN)_6]^{3-/4-}$ in 0.1 M KCl at the various electrodes as well as the CV responses of the FeTSPc-based electrodes in 0.1 M KCl solution without the redox probe.

PABS. This is further confirmed by the Bode plots (Fig. 8) where Au-DMAET-SWCNT-PABS/FeTSPc gave the lowest impedance (Fig. 8a) and lowest phase angle (Fig. 8b). This is not fully understood but may be related to such factors as the SWCNT-PABS acting as nanowires for an efficient electron-conducting mediator for the facile electron transport for the FeTSPc species. Second, the charge storage capability of the modified electrodes (CPE) decreases as Au-DMAET (145 μF cm^{-2}) > Au-DMAET-SWCNT-PABS/

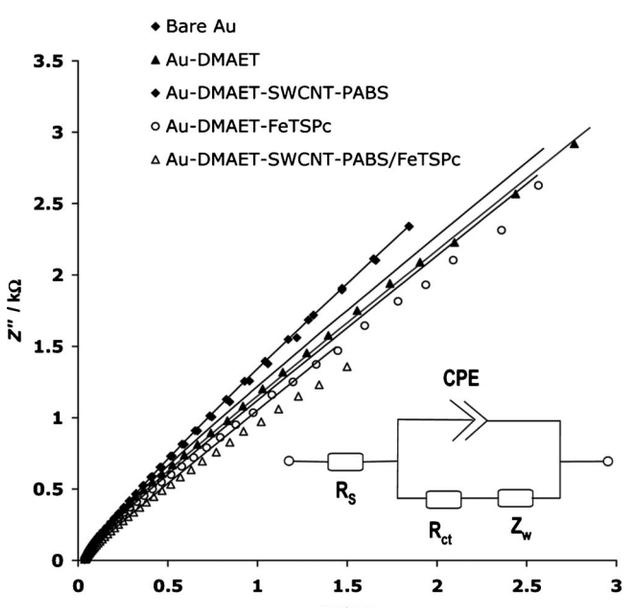

Figure 7. Nyquist plots obtained in $[Fe(CN)_6]^{3-/4-}$ in 0.1 M KCl at the various electrodes. Applied potential = 0.265 V (vs Ag | AgCl, saturated KCl). Inset is the modified Randles' equivalent circuit used in the fitting.

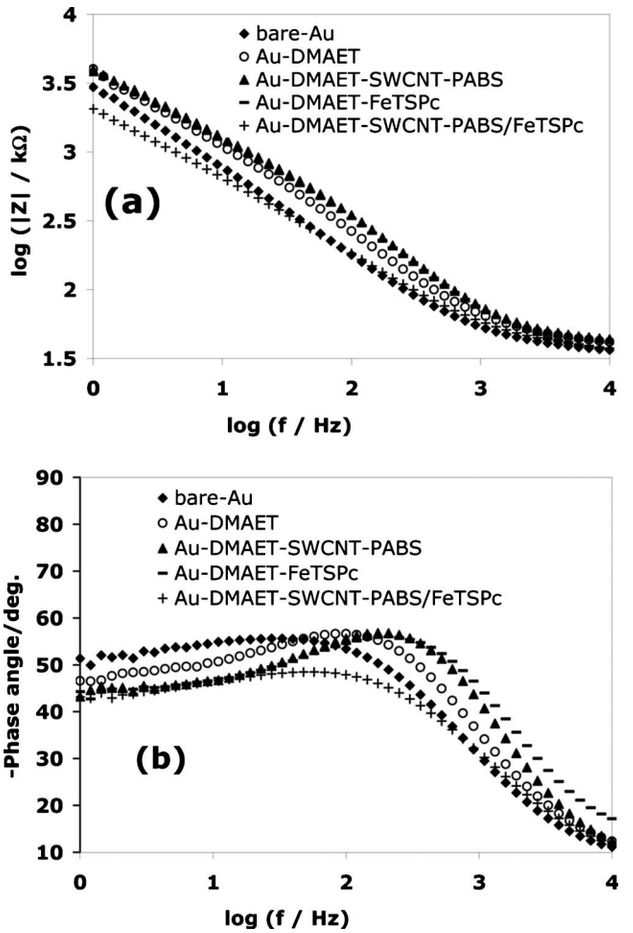

Figure 8. Bode plots [(a) phase angle and (b) log Z vs log f] obtained in $[Fe(CN)_6]^{3-/4-}$ in 0.1 M KCl at the various electrodes. Experimental conditions as in Fig. 7.

FeTSPc (141 μF cm^{-2}) > Au-DMAET-SWCNT-PABS (63 μF cm^{-2}) > Au-DMAET-FeTSPc (60 μF cm^{-2}). This trend is similar, as seen in PBS solution (pH 7.4) studied using CV (Fig. 3), with the difference in value being related to the different electrolyte and techniques used.

The impedance (Z_{CPE}) is defined as[52]

$$Z_{CPE} = \frac{1}{[Q(j\omega)^n]} \quad [6]$$

where Q is the frequency-independent constant relating to the surface electroactive properties, ω is the radial frequency, the exponent n arises from the slope of log Z vs log f (and has values $-1 \leq n \leq 1$). If $n = 0$, the CPE behaves as a pure resistor; $n = 1$, CPE behaves as a pure capacitor, $n = -1$ CPE behaves as an inductor; whereas $n = 0.5$ corresponds to Warburg impedance (Z_w), which is associated with the domain of mass transport control arising from the diffusion of ions to and from the electrode|solution interface. Generally speaking, CPE may occur as a result of several factors,[52-54] including (*i*) the nature of the electrode (e.g., roughness and polycrystallinity), (*ii*) distribution of the relaxation times due to heterogeneities existing at the electrode|electrolyte interface, (*iii*) porosity, and (*iv*) dynamic disorder associated with diffusion. From Table II, $n \approx 1$, suggesting pure capacitive behavior; however, the slopes of the log Z vs log f plot are approximately similar (ca. −0.60) at the midfrequency region, indicative of pseudocapacitive behavior.

Table II. Summary of EIS parameters of the modified electrodes obtained from fitted impedance spectral using the modified Randles equivalent circuit model (Fig. 7 inset).

Electrochemical impedance parameters[a]	Modified gold electrode[b]			
	Au-DMAET	Au-DMAET-SWCNT-PABS	Au-DMAET-FeTSPc	Au-DMAET-SWCNT-PABS/FeTSPc
R_s/Ω cm^2	1.13 (1.88)	1.17 (2.68)	1.01 (2.24)	1.02 (2.55)
R_{ct}/Ω cm^2	1.40 (12.95)	1.33 (15.90)	1.25 (9.11)	0.72 (10.35)
CPE/μF cm^{-2}	145.38 (11.89)	63.08 (16.43)	60.00 (14.81)	140.77 (24.13)
n	0.94 (1.42)	0.99 (1.77)	0.99 (1.57)	0.91 (2.78)
$Z_w/\mu\Omega$ cm^2	2.49 (4.38)	2.41 (1.51)	2.70 (1.22)	4.86 (1.69)
k^o/cm s^{-1}	0.19 $\pm$ 0.03	0.20 $\pm$ 0.03	0.21 $\pm$ 0.02	0.37 $\pm$ 0.04

[a] Value in parenthesis is the estimated percent errors in fitting the experimental impedance spectra.
[b] The data for bare gold electrode were the same as previously reported (Ref. 28) and were not repeated here.

CPE is preferred for a real application situation. However, the CPE in this work could be replaced with the ideal double layer capacitance (C_{dl}) in the modeling circuit, also yielding approximately the same R_s and R_{ct} results. The explanation of this observation may be found from the relationship between C_{dl} and CPE. It has been elegantly described by Orazem and Tribollet[53] that frequency dispersion leading to CPE behavior occurs as a result of the distribution of time constants along either the area of the electrode surface [involving a two-dimensional (2D) aspect of the electrode] or along the axis normal to the electrode surface [involving a three-dimensional (3D) surface]. A 2D distribution presents itself as an ideal resistance–capacitance behavior, meaning that impedance measurements are very useful in distinguishing whether the observed global CPE behavior is due to a 2D or 3D distribution or both. Thus, the observed impedimetric behavior seen at the modified electrodes likely involves 2D and 3D distributions. Also, the phase angles seen on the Bode plots [i.e., phase angle (θ) vs log f, (Fig. 8)] are in the range of 48–56°, which are less than the 90° expected of an ideal capacitive behavior, thus further confirming the presence of the 2D distribution arising from CPE behavior and the pseudocapacitive nature of the modified electrodes.

Conclusions

The stable integration of a highly water-soluble, redox-active electrocatalyst, the FeTSPc complex, on an electrode surface is crucial for its fundamental studies and potential applications in heterogeneous electrocatalysis and sensing. The combined integration of FeTSPc with highly electronic conducting materials such as SWCNT-PABS is important to enhance the redox activity and electrocatalytic properties of metallophthalocyanine. Using CV and impedance spectroscopy, we have clearly shown that the water-soluble, sulfonated redox-active species (FeTSPc and SWCNT-PABS) could be stably confined onto a gold electrode via electrostatic interaction chemistry with a positively charged SAM of DMAET. The nanothin films of these redox-active species exhibited excellent electrochemical stability and enhanced heterogeneous electron transfer kinetics of an outer sphere redox probe ($[Fe(CN)_6]^{4-}/[Fe(CN)_6]^{3-}$). This result thus suggests that the proposed fabrication strategy could potentially be extended to other water-soluble metallophthalocyanines and related organometallic complexes.

Acknowledgments

We thank NRF for their support through the "Unlocking the future," "NNEP," and "Nanotechnology flagship" funding programmes. B.O.A. thanks NRF for Scarce Skill Postdoctoral Fellowship award. J.P. thanks Project AuTEK (MinTEK and Gold Fields) and NRF for Ph.D. scholarship.

Council for Scientific and Industrial Research assisted in meeting the publication costs of this article.

References

1. R. G. Nuzzo and D. L. Allara, *J. Am. Chem. Soc.*, **105**, 4481 (1983).
2. B. O. Agboola and K. I. Ozoemena, *Phys. Chem. Chem. Phys.*, **10**, 2399 (2008).
3. N. S. Mathebula, J. Pillay, G. Toschi, J. A. Verschoor, and K. I. Ozoemena, *Chem. Commun. (Cambridge)*, **2009** 3345.
4. K. I. Ozoemena and T. Nyokong, *J. Electroanal. Chem.*, **579**, 283 (2005).
5. B. Agboola, K. I. Ozoemena, P. Westbroek, and T. Nyokong, *Electrochim. Acta*, **52**, 2520 (2007).
6. F. N. Crespilho, F. Huguenin, V. Zucolotto, P. Olivi, F. C. Nart, and O. N. Oliveira, Jr., *Electrochem. Commun.*, **8**, 348 (2006).
7. F. N. Crespilho, V. Zucolotto, C. M. A. Brett, O. N. Oliveira, Jr., and F. C. Nart, *J. Phys. Chem. B*, **110**, 17478 (2006).
8. J. R. Siqueira, Jr., L. H. S. Gasparotto, O. N. Oliveira, Jr., and V. Zucolotto, *J. Phys. Chem. C*, **112**, 9050 (2008).
9. S. S. Fan, M. G. Chapline, and N. R. Franklin, *Science*, **283**, 512 (1999).
10. Z. W. Pan, S. S. Xie, and L. Lu, *Appl. Phys. Lett.*, **74**, 3152 (1999).
11. K. I. Ozoemena and T. Nyokong, *J. Electroanal. Chem.*, **6**, 1192 (2003).
12. B. Agboola, K. I. Ozoemena, and T. Nyokong, *J. Mol. Catal. A: Chem.*, **248**, 84 (2006).
13. F. Bedioui, S. Griveau, T. Nyokong, A. J. Appleby, C. A. Caro, M. Gulppi, G. Ochoa, and J. H. Zagal, *Phys. Chem. Chem. Phys.*, **9**, 3383 (2007).
14. B. Agboola, P. Westbroek, K. I. Ozoemena, and T. Nyokong, *Electrochem. Commun.*, **9**, 310 (2007).
15. K. I. Ozoemena, T. Nyokong, D. Nkosi, I. Chambrier, and M. J. Cook, *Electrochim. Acta*, **52**, 4132 (2007).
16. B. O. Agboola, K. I. Ozoemena, T. Nyokong, T. Fukuda, and N. Kobayashi, *Carbon*, **48**, 763 (2010).
17. J. R. Reynolds, M. Pyo, and Y.-J. Qiu, *J. Electrochem. Soc.*, **141**, 35 (1994).
18. K. I. Ozoemena and T. Nyokong, *Electrochim. Acta*, **51**, 5131 (2006).
19. K. I. Ozoemena, D. Nkosi, and J. Pillay, *Electrochim. Acta*, **53**, 2844 (2008).
20. K. I. Ozoemena and T. Nyokong, *J. Chem. Soc. Dalton Trans.*, **2002**, 1806.
21. *Phthalocyanines: Properties and Applications*, C. C. Leznoff and A. B. P. Lever, Editors, VCH, New York (1989).
22. K. I. Ozoemena and T. Nyokong, in *Encyclopedia of Sensors*, Vol. 3, Chap. E,C. A. Grimes, E. C. Dickey, and M. V. Pishko, Editors, p. 157, American Scientific, Valencia, CA (2006).
23. *The Porphyrin Handbook*, K. M. Kadish, K. M. Smith, and R. Guilard, Editors, Academic Press, Boston, MA (2003).
24. J. R. Siqueira, Jr., L. H. S. Gasparotto, F. N. Crespilho, A. J. F. Carvalho, V. Zucolotto, and O. N. Oliveira, Jr., *J. Phys. Chem. B*, **110**, 22690 (2006).
25. J. R. Siqueira, Jr., F. N. Crespilho, V. Zucolotto, and O. N. Oliveira, Jr., *Electrochem. Commun.*, **9**, 2676 (2007).
26. J. Francisco Silva, S. Griveau, C. Richard, J. H. Zagal, and F. Bedioui, *Electrochem. Commun.*, **9**, 1629 (2007).
27. K. I. Ozoemena, J. Pillay, and T. Nyokong, *Electrochem. Commun.*, **8**, 1391 (2006).
28. J. Pillay and K. I. Ozoemena, *Electrochim. Acta*, **54**, 5053 (2009).
29. J. Pillay and K. I. Ozoemena, *Chem. Phys. Lett.*, **441**, 72 (2007).
30. J. H. Zagal, S. Griveau, K. I. Ozoemena, T. Nyokong, and F. Bedioui, *J. Nanosci. Nanotechnol.*, **9**, 2201 (2009).
31. J. H. Weber and D. H. Busch, *Inorg. Chem.*, **4**, 472 (1965).
32. B. A. Boukamp, *Solid State Ionics*, **20**, 31 (1986).
33. R. G. Compton and C. E. Banks, *Understanding Voltammetry*, World Scientific, Singapore (2007).
34. A. J. Bard and L. R. Faulkner, *Electrochemical. Methods Fundamentals and Applications*, 2nd ed., John Wiley & Sons, Hoboken, NJ (2001).
35. J. M. Campiña, A. Martins, and F. Silva, *J. Phys. Chem. C*, **111**, 5351 (2007).
36. S. M. Rosendahl and I. J. Burgess, *Electrochim. Acta*, **53**, 6759 (2008).
37. J. Pillay, B. O. Agboola, and K. I. Ozoemena, *Electrochem. Commun.*, **11**, 1292 (2009).
38. A. B. P. Lever, E. L. Milaeva, and G. Speier, in *Phthalocyanines: Properties and Applications*, Vol. 3, Chap. 1, C. C. Leznoff and A. B. P. Lever, Editors, p. 1, VCH, New York (1993).

39. H. O. Finklea, in *Electroanalytical Chemistry*, Vol. 19, A. J. Bard and I. Rubinstein, Editors, p. 109, Marcel Dekker, New York (1996).
40. H. O. Finklea, in *Encyclopedia of Analytical Chemistry, Applications, Theory and Instrumentations*, Vol. 11, R. A. Meyers, Editor, p. 10090, John Wiley & Sons, Chichester (2000).
41. H. O. Finklea, *J. Am. Chem. Soc.*, **114**, 3173 (1992).
42. H. O. Finklea, M. S. Ravenscroft, and D. A. Snider, *Langmuir*, **9**, 223 (1993).
43. J. Liu, M. N. Paddon-Row, and J. J. Gooding, *J. Phys. Chem. B*, **108**, 8460 (2004).
44. J. J. Gooding, A. Chou, J. Liu, D. Losic, J. G. Shapter, and D. B. Hibbert, *Electrochem. Commun.*, **9**, 1677 (2007).
45. B. S. Flavel, J. Yu, A. V. Ellis, and J. G. Shapter, *Electrochim. Acta*, **54**, 3191 (2009).
46. D. Nkosi, J. Pillay, K. I. Ozoemena, K. Nouneh, and M. Oyama, *Phys. Chem. Chem. Phys.*, **12**, 604 (2010).
47. Y.-H. Tse, P. Janda, H. Lam, W. J. Pietro, and A. B. P. Lever, *J. Porphyr. Phthalocyanines*, **1**, 3 (1997).
48. M. P. Somashekarappa, J. Keshavaya, and S. Sampath, *Pure Appl. Chem.*, **74**, 1609 (2002).
49. J. Jiang and A. Kucernak, *Synth. Met.*, **114**, 209 (2000).
50. B.-Y. Chang, S.-Y. Hong, J.-S. Yoo, and S.-M. Park, *J. Phys. Chem. B*, **110**, 19386 (2006).
51. A. Bezegh and J. Janata, *J. Electrochem. Soc.*, **133**, 2087 (1986).
52. E. Barsoukov and J. R. Macdonald, *Impedance Spectroscopy: Theory Experiment, and Applications*, 2nd ed., John Wiley & Sons, Hoboken, NJ (2005).
53. M. E. Orazem and B. Tribollet, *Electrochemical Impedance Spectroscopy*, John Wiley & Sons, Hoboken, NJ (2008).
54. V. Ganesh, S. Pitchumani, and V. Lakshminarayanan, *J. Power Sources*, **158**, 1523 (2006).